Hindawi Publishing Corporation
Journal of Nanomaterials
Volume 2006, Article ID 87326, Pages 1–7
DOI 10.1155/JNM/2006/87326

Visible Light Photocatalysis via CdS/TiO_2 Nanocomposite Materials

Sesha S. Srinivasan, Jeremy Wade, and Elias K. Stefanakos

Clean Energy Research Center, College of Engineering, University of South Florida, Tampa, FL 33620, USA

Received 17 January 2006; Revised 8 August 2006; Accepted 9 August 2006

Nanostructured colloidal semiconductors with heterogeneous photocatalytic behavior have drawn considerable attention over the past few years. This is due to their large surface area, high redox potential of the photogenerated charge carriers, and selective reduction/oxidation of different classes of organic compounds. In the present paper, we have carried out a systematic synthesis of nanostructured CdS-TiO_2 via reverse micelle process. The structural and microstructural characterizations of the as-prepared CdS-TiO_2 nanocomposites are determined using XRD and SEM-EDS techniques. The visible light assisted photocatalytic performance is monitored by means of degradation of phenol in water suspension.

1. INTRODUCTION

Anatase TiO_2 is the most widely used semiconductor photocatalyst for an effective decomposition of organic compounds in air and water under UV light irradiation, with wavelength shorter than 387 nm [1, 2]. The major problem is that only about 4% of the solar spectrum falls in this UV range. The efficient use of sunlight becomes an appealing challenge for developing photocatalysts [3–5]. One approach for achieving this objective is to sensitize TiO_2 by using a narrow band gap semiconductor with a higher conduction band than that of TiO_2. CdS with band gap energy of 2.5 eV is considered to be one of the many sensitizers used for large band gap semiconductors because of the ideal position of its conduction and valence band edges. CdS alone, however, shows negligible photocatalytic activity because of its instability and rapid electron-hole pair (EHP) recombination rates. Studies have proven that with the appropriate particle interaction, CdS-TiO_2 nanocomposites can efficiently decompose organics such as phenol and methylene blue under visible light irradiation less than 495 nm [6–8].

The reaction as shown in Figure 1 occurs when a CdS particle is excited by a photon with a wavelength less than 495 nm. An EHP is formed, and subsequently the photogenerated electron is quickly transferred to the conduction band of a coupled TiO_2 particle that has a conduction band edge more positive than the CdS particle ($\sim$ 0.5 eV). The photogenerated hole in the quantum-sized CdS particle can theoretically migrate to the surface and participate in the oxidation of adsorbed organics. The electrons that are transferred to the conduction band of TiO_2 have no holes to recombine with and therefore participate in reduction reactions according to the conduction band energy level of TiO_2. In order to establish a quantum size effect, one must have to synthesize extremely small particles of the order of the excitonic diameter and to stabilize them against further growth. Reverse micelle process provides a controlled environment to achieve this goal.

Reverse micelles are thermodynamically stable structures which consist of a nanometer-sized spherical water core that is encapsulated by surfactant molecules in a nonpolar medium. They have been used to synthesize semiconductors, metals, and other inorganic crystallites [9–11]. Interparticle electron transfer between size quantized CdS and TiO_2 semiconductor nanoclusters for the photocatalysis and hydrogen production applications is reported in recent years [12–19].

In the present study, we have carried out the successful formulation of CdS-TiO_2 nanocomposite via reverse micelle process and studied their structural, microstructural, UV-Vis spectral characteristics and visible light photocatalytic behavior.

2. EXPERIMENTAL DETAILS

2.1. Materials and method

The chemicals used for the synthesis of CdS-TiO_2 nanocomposite are of the purest quality and are used as received:

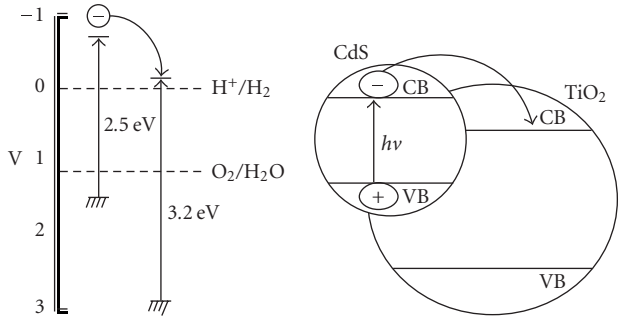

Figure 1: CdS-TiO_2 nanocomposite with band edge energy levels.

cadmium perchlorate hydrate ($Cd(ClO_4)_2.\times H_2O$), titanium (IV) isopropoxide ($Ti(OCH_2CH_2CH_3)_4$), sodium sulfide (Na_2S), Aerosol-OT, solvents such as isooctane, 2-proponal, *n*-heptane are obtained from Sigma-Aldrich. Initially the reverse micelles are prepared by optimizing the surfactant to water mole ratio (w_0) in nonpolar medium (say, isooctane);

$$w_0 = [\text{AOT}]/[H_2O]. \quad (1)$$

In the next step, adding 1 M $Cd(ClO_4)_2. \times H_2O$ to this reverse micelle to form microemulsion "A." Similarly, the microemulsion "B" is formed by adding 0.1 M Na_2S to a separate reverse micelle solution. Mixing the microemulsions A and B with vigorous stirring at room temperature thus produces CdS yellowish microemulsion "C." Another microemulsion "D" is formed by adding 1 M $Ti(OPr)_4$/2-propanol in separate reverse micelle and stirred continuously for 1 hour. The water to alkoxide ratio (h) have been varied and optimized for the TiO_2 precipitation,

$$h = [H_2O]/[Ti(OPr)_4]. \quad (2)$$

The microemulsions of "C" and "D" are finally mixed and vigorously stirred to form CdS-Xwt.% TiO_2 (x= 5, 10, 50). The CdS-TiO_2 precipitate obtained is then washed couple of times with DI water, ethanol, and acetone to remove the surfactant. The amorphous nanocomposite of CdS-TiO_2 is calcined at 500°C under the flow of N_2 for 3 hours.

2.2. Structural and microstructural characterization

The structural characterization for the phase identification and particle size analysis has been carried out using Philips X'pert pro powder X-ray diffractometer with CuKα radiation ($\lambda = 1.54060\,\text{Å}$). The incident and diffraction slit width used for all the experiments are 1° and 2°, respectively, and the incident beam mask used corresponds to 10 mm. The XRD profile analysis and particle sizes have been calculated using PANalytical X'pert Highscore software version 1.0 e.

The microstructural characterizations such as surface morphology and chemical composition were performed using scanning electron microscope SEM (Hitachi S-800) both in imaging and EDS modes. Genesis software has been used to analyze the microstructures and elemental composition of the CdS-TiO_2 nanocomposites.

2.3. BET surface area measurements

Catalysts and photocatalysts are often characterized by their interaction with gases. At low temperatures, nonreactive gases (nitrogen, argon, krypton, etc.) are *physi*sorbed by the surface. Through gas physisorption the total surface area of the sample can be calculated by the BET method. The ChemBET 3000 from Quantachrome Instruments has been employed to determine the surface area and a pore size distribution of the pure TiO_2, pure CdS, and CdS-TiO_2 nanocomposites. A known amount of sample ($\sim$ 100 mg) was placed in a glass tube and the sample was outgassed at 300°C for 5 hours. Multipoint BET method using nitrogen as the adsorbate gas, the isotherm has been measured at 77 K.

2.4. UV-Vis transmittance spectroscopy

The transmittance measurement is performed by UV-Vis spectrometer. The powder samples of pure TiO_2 and CdS-TiO_2 nanocomposite are made into slurry by dissolving it in (Acetylacetone + H_2O + Triton X-100) solution. Thus obtained slurry was spin coated at 4000 rpm on to the glass slide for UV-Vis spectrum studies. The homogeneous films obtained from spin coating samples were then subjected to UV-Vis spectroscopy measurements in transmittance and absorption modes using an Ocean Optics USB2000 fiber optic spectrometer.

2.5. Photocatalytic reactor testing

Photocatalytic experiments using visible light and a combination of UV-A and visible light were performed using a single lamp and an annular reflector to provide irradiation to all sides of the reaction vessel as shown in Figure 2. The immersion well was used as a means of concentrating the aqueous solution to the perimeter of the reaction vessel to optically optimize the system. A 1000 W metal halide lamp was experimentally chosen, since it adequately replicated both the pattern and intensity peaks of the solar spectrum more accurately than other visible sources such as high-pressure sodium and fluorescent lamps.

The metal halide spectrum, as shown in Figures 3(a) and 3(b), was found to contain sufficient UV-A radiation in the range of 350 nm–400 nm to serve as both a UV-A and visible light source. For photocatalytic experiments using visible light region, a longpass UV filter provided by Edmund Optics was used to cut off the wavelengths shorter than 400 nm, at a cost of approximately 8% attenuation at wavelengths greater than 400 nm. The system was cooled from 110°C to 70°C using ventilation provided by three fans inputting and removing air from the surface of the lamp and inside the reactor.

2.6. Phenol degradation by UV-Vis spectroscopy measurement

Photocatalytic phenol degradation experiments were conducted using the following procedure. A solution of deionized water, phenol, and the catalyst under test were mixed

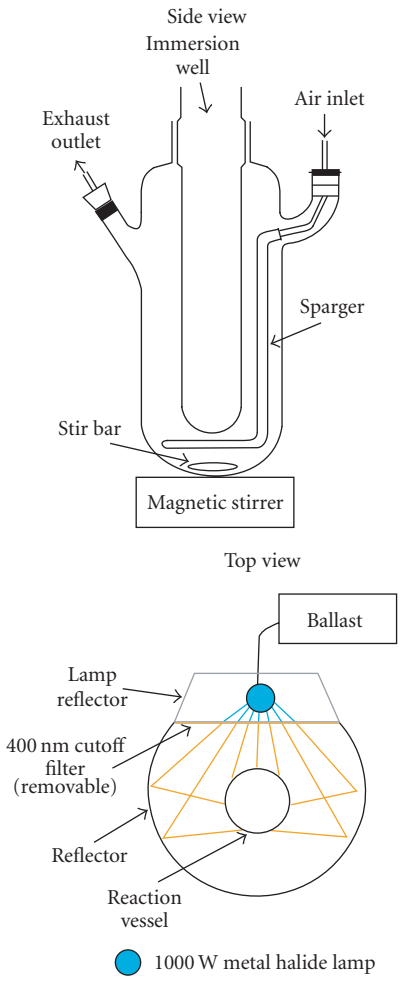

Figure 2: UV-Vis/visible light photocatalytic reactor used for phenol degradation studies.

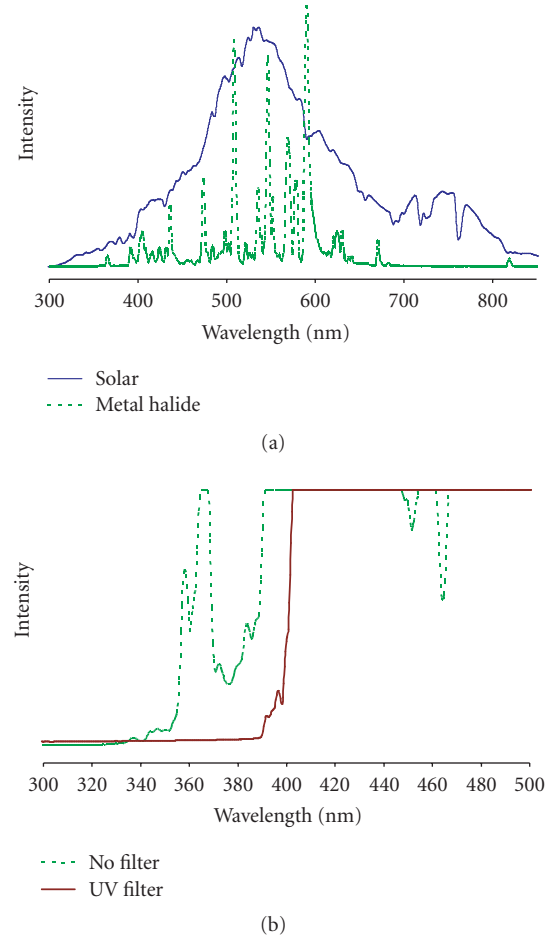

Figure 3: (a) UV-Vis metal halide spectrum compared to solar irradiation and (b) effects of UV-cutoff filter on metal halide irradiation pattern.

using magnetic stirring, and air was injected to scavenge photogenerated electrons and also to help suspend the catalyst. The phenol concentration in all experiments was 40 ppm which was selected as a value large enough to accurately measure using absorption measurements and small enough to degrade within hours when exposed to an efficient photocatalyst. Air was dispersed in the aqueous solution through a 12-inch rod sparger and was used in place of pure O_2 to simulate real-world experimental conditions. Periodic 1.5 mL samples were retrieved from the reaction vessel in desired time increments and placed in Eppendorf microcentrifuge tubes for analysis of the photocatalytic degradation of phenol. The nanoparticle catalysts were separated from the phenol and water mixtures by centrifuging the Eppendorf tubes for 10 minutes at 4000 rpm and 3220 rcf using an Eppendorf 5810 R centrifuge. UV-Vis spectroscopy using an Ocean Optics USB2000 fiber optic spectrometer was used to analyze the degradation of phenol with respect to time by monitoring the intensity of the absorption peak of phenol located at 268.63 nm. Phenol degradation was determined with respect to its initial concentration, and therefore all degradation plots are normalized based on C/C_0 values which are interpreted as the concentration at the measured time divided by the initial concentration.

3. RESULTS AND DISCUSSION

3.1. Structural characterization

Figure 4 represents the X-ray diffraction patterns of (a) pure CdS nanoparticle (b) pure TiO_2 anatase and (c) CdS-50 wt.% TiO_2 nanocomposite prepared via reverse micelle process. No impurity peaks from the precursor ingredients such as cadmium perchlorate hydrate and sodium sulfide are observed for the pure TiO_2 and CdS as shown in Figures 4(a) and 4(b). However, for the CdS-50 wt.% TiO_2 nanocomposite, impurity peaks due to sodium perchlorate ($NaClO_4$) (see Figure 4(c)) are observed at the angle of orientations 22.4098° and 30.21111°. This may be due to the starting precursor reactions, which needs further filtration and purification. Also from these X-ray patterns, it is easily discernable that there exist two different grain sizes of the nanocomposite

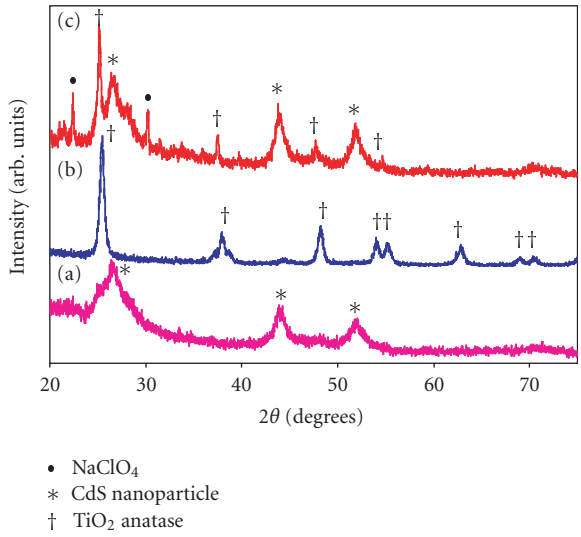

FIGURE 4: X-ray diffraction patterns of pure CdS, pure TiO_2 anatase, and CdS-50 wt.% TiO_2 nanocomposite prepared via reverse micelle process.

mixture due to CdS nanoparticle and TiO_2 anatase. We have calculated the average crystallite sizes from the X-ray diffraction patterns (Figure 4) according to Scherrer's equation and given in Table 1. The nanocomposite CdS-50 wt.% TiO_2 exhibits the larger crystallites when compared to either pure TiO_2 or pure CdS. This is due to high temperature (500°C) calcination involved after the composite formation in reverse micelle process.

3.2. Microstructural and chemical characterization

The microstructural characterization of the CdS-50 wt.% TiO_2 nanocomposite is carried out via scanning electron microscopy. Figures 5(a) and 5(b) show the SEM image and EDS spectrum of the CdS coupled TiO_2 nanocomposite structure. Reverse micelle process of preparing semiconductor nanocomposite yields homogeneous particles, thus improves the interparticle electron transfer from high-lying conduction band semiconductor with a small band gap (e.g., CdS ∼ 2.5 eV) to low-lying conduction band semiconductor with a large band gap (e.g., TiO_2 ∼ 3.2 eV). The EDS profile shows correct stoichiometry of CdS to TiO_2 in the nanocomposite structure. The atomic ratio of Cd and Ti in the nanocomposite structure was 3 at.% : 9 at.%. obtained from the SEM-EDS spectrum as shown in Figure 5(b).

The growth of intergrain boundaries between the CdS and TiO_2 nanostructures and the particle size varies with the experimental parameters such as water-to-surfactant ratio (w_0), water-to-alkoxide ratio (h), pH concentration of obtained solution, ratio of CdS to TiO_2 precursors, and calcination temperatures. The optimized parameters for the reverse micelle nanocomposite CdS-50 wt.% TiO_2 structure are given in Table 2. The standards for determining the optimizing conditions given in Table 2 are explained below.

The molar ratio of H_2O to surfactant AOT (w_0) was varied as 2, 4, 6, 8, and 10. The reverse micelle and gelation formation rates are highly controlled by varying this ratio. Rapid gelation with larger crystallites occurred during the higher molar ratio of water to surfactant, (e.g., $w_0 = 8, 10$) whereas slow gelations are due to the lower value of w_0 (e.g., 2, 4). An optimum value of $[AOT]/[H_2O] = 6$ was found and used for the further experiments. Similarly, the ratio of $[H_2O]$/[Ti-alkoxide] was optimized to obtain appropriate concentration of TiO_2. The acidic/basic nature of the reverse micelle CdS-TiO_2 is easily controlled by decreasing or increasing the pH value. The rapid precipitation effect was monitored and controlled by suitably adjusting the pH to 9. Thus obtained CdS-TiO_2 nanocomposite was then calcined at different temperatures under flowing N_2 atmosphere. Increasing the calcination temperature above 500°C, the appearance of rutile TiO_2 structure is inevitable and thus lowers the photocatalytic effect of CdS-TiO_2 nanocomposites. Calcination temperature below 500°C yields poor crystalline structure of CdS and TiO_2. Hence the optimum calcination temperature was found to be 500°C for rest of the experiments.

3.3. UV-Vis spectral response

The UV-Vis transmittance spectral response for the pure TiO_2 and CdS-50 wt.% TiO_2 nanocomposite is shown in Figure 6. The onset of transmittance starts below 350 nm and a sharp transition occurred at around 380 nm for the pure TiO_2 anatase structure. Whereas for the case of CdS-50 wt.% TiO_2 nanocomposite prepared by reverse micelle process, the spectral curve extends to the visible light region with the onset value corresponding to 490 nm. The absorption edge of TiO_2 in CdS-TiO_2 nanocomposites observed above 400 nm indicates a significant "*blue shift*" of the bandgap energy compared to pristine TiO_2. The quantum-sized effect of CdS in the nanocomposite structure seems plausible explanation for this "*blue* shift" effect [20]. However, in the present study, the quantum CdS is not observed due to the coalescent or agglomeration of nanoparticles in the reverse micelle process. This may suggest that the nanocomposite coupled semiconductor (CdS-50 wt.% TiO_2) is expected to increase photogenerated charge carriers under the irradiation of visible light. It is noteworthy to mention that the absorption spectrum due to TiO_2 is not present in the CdS-TiO_2 nanocomposite films due to the different film thickness between TiO_2 and CdS nanoparticles. Besides, the concentration of TiO_2 also affects the optical absorption of CdS-TiO_2 nanocomposites in the UV range.

3.4. Photodegradation of phenol in water suspension

Photoactivity of the as-prepared CdS-Xwt.% TiO_2 nanocomposite materials is determined by the degradation of phenol in water suspension under visible light irradiation. Photocatalytic experiments using purely visible light, a long-pass UV filter provided by Edmund Optics was used to cut off the wavelengths below 400 nm. Phenol is chosen as a

Table 1: Average crystallite sizes of CdS, TiO_2 anatase, and CdS-50 wt.% TiO_2 nanocomposite.

No.	Photocatalyst material	Average crystallite size	Surface area, BET
(1)	Pure CdS (Figure 4(a))	11.9 nm	36 m^2/g
(2)	Pure TiO_2 anatase (Figure 4(b))	37.9 nm	50 m^2/g
(3)	CdS-TiO_2 nanocomposite (Figure 4(c))	CdS ∼ 18.1 nm TiO_2 ∼ 59.9 nm	24 m^2/g

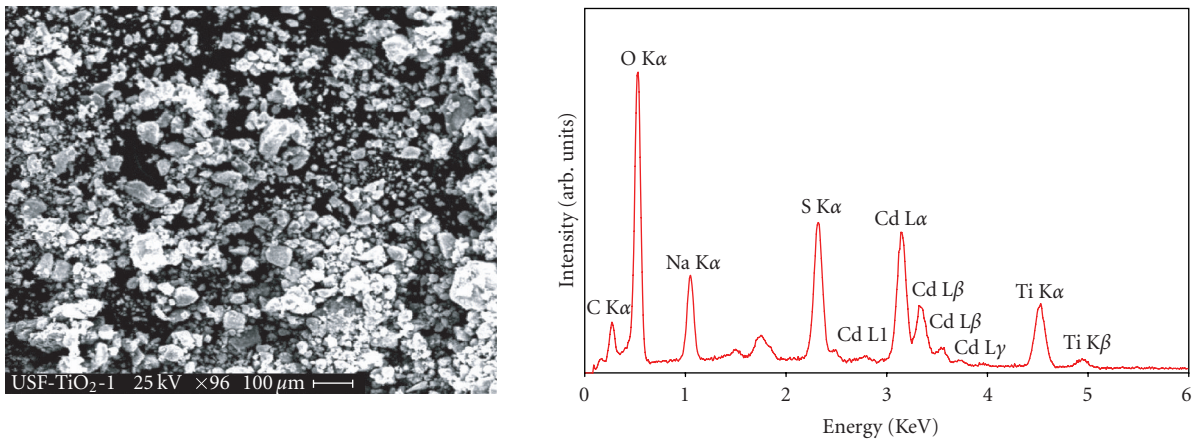

Figure 5: (a) SEM microstructure image of CdS-50 wt.% TiO_2 nanocomposite prepared via reverse micelle and (b) SEM-EDS spectrum of CdS-50 wt.% TiO_2 nanocomposite prepared via reverse micelle.

Table 2: Experimental parameters for the optimized CdS-50 wt.% TiO_2 nanocomposite material.

No.	Experimental parameter	Optimized value
(1)	Water-to-surfactant ratio, w_0	6
(2)	Water-to-alkoxide precursor ratio, h	4
(3)	pH	9
(4)	Calcination temperature (N_2 atmosphere)	500°C

test degradant for its photoactivity behavior. The primary reason is that phenol is an ideal degradant for visible light photocatalysis measurements because it absorbs only UV-C radiation with an absorption peak between 265 nm and 270 nm. This implies that it will not be susceptible to photolysis when irradiated by UV-A and visible light. Phenol is also a test degradant that exhibits application, since it is a common contaminant of industrial effluents. Photocatalytic oxidation of phenolic compounds in industry has been suggested to replace other processes such as activated carbon absorption, chemical oxidation, biological treatment, wet oxidation, and ozonolysis [21]. A third reason phenol is used is that the photooxidation of phenolic compounds illuminated TiO_2 surfaces has been widely studied and the reaction kinetics are found to be first order following the well established Langmuir-Hinshelwood equation [22, 23].

The normalized phenolic concentrations (C/C_0) at regular intervals for the CdS-Xwt.% TiO_2 nanocomposite have been plotted in Figure 7.

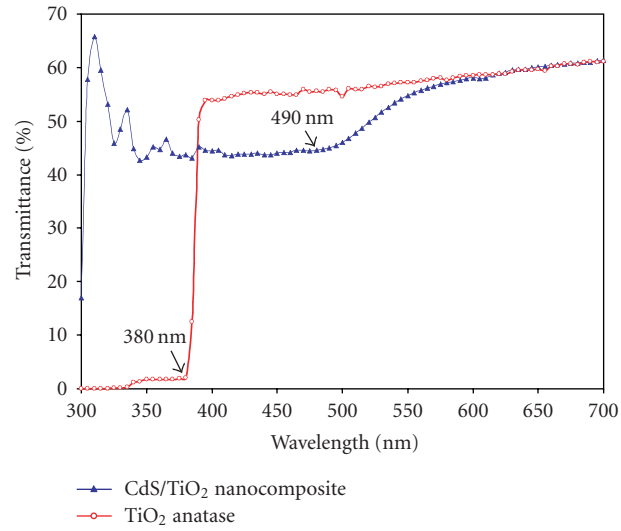

Figure 6: UV-Vis spectral responses for pure TiO_2 and CdS-TiO_2 nanocomposite.

There is no direct correlation of rate of degradation and the CdS content was observed in the CdS-TiO_2 nanocomposite structure. However, the photodegradation of phenol concentration up to 40% is achieved in the CdS-50 wt.% TiO_2 nanocomposite material. Great efforts are presently being carried out to tailor the nanocomposite system by optimizing

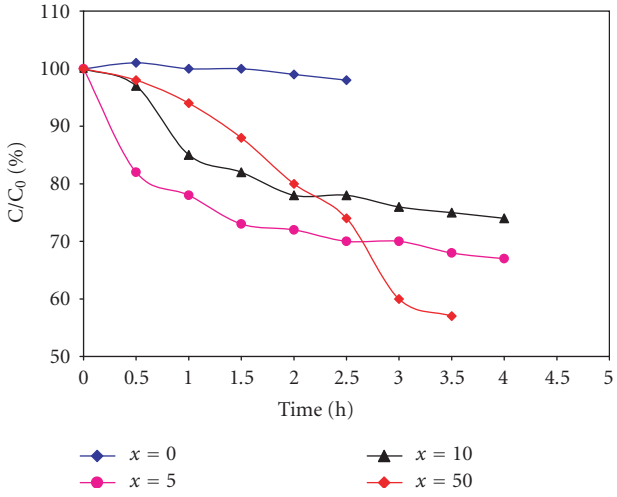

Figure 7: Phenol degradation of CdS-Xwt.% TiO_2.

the experimental conditions and solve the corrosion behavior of CdS for the effective photoactivity under visible light irradiations. We will also attempt to synthesize these systems by mechanochemical process employing high energy planetary milling and the results will be forthcoming.

4. CONCLUSIONS

We have systematically carried out the synthesis of pure TiO_2, pure CdS and CdS coupled TiO_2 nanocomposite by employing reverse micelle process. The X-ray phase analysis of these systems shows evidence for the formation of heterojunction CdS-Xwt.% TiO_2 nanocomposite structure with average crystallite sizes ranging from 18 nm to 60 nm. The microstructural investigation of the nanocomposite envisages the correct stoichiometry of CdS to TiO_2 and homogeneous surface morphology. The surface-coated CdS and TiO_2 anatase nanocomposite extends the absorption band edge in the visible region as observed from the UV-Vis measurements. The as-synthesized nanocomposite materials exhibit better photoactivity under visible light irradiation than that of pure TiO_2.

ACKNOWLEDGMENTS

Authors wish to thank the Nanomaterials and Nanomanufacturing Research Center at University of South Florida for extensive use of X-ray diffraction and SEM facilities. Financial support from DOE and Center for Biological Defense are gratefully acknowledged.

REFERENCES

[1] N. Serpone and E. Pelizzetti, *Photocatalysis: Fundamentals and Applications*, John Wiley & Sons, New York, NY, USA, 1989.

[2] M. A. Fox and M. T. Dulay, "Heterogeneous photocatalysis," *Chemical Reviews*, vol. 93, no. 1, pp. 341–357, 1993.

[3] R. Asahi, T. Morikawa, T. Ohwaki, K. Aoki, and Y. Taga, "Visible-light photocatalysis in nitrogen-doped titanium oxides," *Science*, vol. 293, no. 5528, pp. 269–271, 2001.

[4] M. R. Hoffmann, S. T. Martin, W. Choi, and D. W. Bahnemann, "Environmental applications of semiconductor photocatalysis," *Chemical Reviews*, vol. 95, no. 1, pp. 69–96, 1995.

[5] S. Yin and T. Sato, "Synthesis and photocatalytic properties of fibrous titania prepared from protonic layered tetratitanate precursor in supercritical alcohols," *Industrial and Engineering Chemistry Research*, vol. 39, no. 12, pp. 4526–4530, 2000.

[6] W. Chengyu, S. Huamei, T. Ying, Y. Tongsuo, and Z. Guowu, "Properties and morphology of CdS compounded TiO_2 visible-light photocatalytic nanofilms coated on glass surface," *Separation and Purification Technology*, vol. 32, no. 1–3, pp. 357–362, 2003.

[7] A. Kumar and A. K. Jain, "Photophysics and photochemistry of colloidal CdS-TiO_2 coupled semiconductors—photocatalytic oxidation of indole," *Journal of Molecular Catalysis A: Chemical*, vol. 165, no. 1-2, pp. 265–273, 2001.

[8] K. R. Gopidas, M. Bohorquez, and P. V. Kamat, "Photophysical and photochemical aspects of coupled semiconductors: charge-transfer processes in colloidal cadmium sulfide-titania and cadmium sulfide-silver(I) iodide systems," *The Journal of Physical Chemistry*, vol. 94, no. 16, pp. 6435–6440, 1990.

[9] P. Lianos and J. K. Thomas, "Cadmium sulfide of small dimensions produced in inverted micelles," *Chemical Physics Letters*, vol. 125, no. 3, pp. 299–302, 1986.

[10] M. L. Steigerwald, A. P. Alivisatos, J. M. Gibson, et al., "Surface derivatization and isolation of semiconductor cluster molecules," *Journal of the American Chemical Society*, vol. 110, no. 10, pp. 3046–3050, 1988.

[11] V. Arcoleo and V. Turco Liveri, "AFM investigation of gold nanoparticles synthesized in water/AOT/n-heptane microemulsions," *Chemical Physics Letters*, vol. 258, no. 1-2, pp. 223–227, 1996.

[12] P. A. Sant and P. V. Kamat, "Interparticle electron transfer between size-quantized Cds and TiO_2 semiconductor nanoclustersy," *Physical Chemistry Chemical Physics*, vol. 4, no. 2, pp. 198–203, 2002.

[13] J. C. Yu, L. Wu, J. Lin, P. Li, and Q. Li, "Microemulsion-mediated solvothermal synthesis of nanosized CdS-sensitized TiO_2 crystalline photocatalyst," *Chemical Communications*, vol. 9, no. 13, pp. 1552–1553, 2003.

[14] Y. Bessekhouad, D. Robert, and J. V. Weber, "Bi_2S_3/TiO_2 and CdS/TiO_2 heterojunctions as an available configuration for photocatalytic degradation of organic pollutant," *Journal of Photochemistry and Photobiology A: Chemistry*, vol. 163, no. 3, pp. 569–580, 2004.

[15] E. Hao, B. Yang, J. Zhang, X. Zhang, J. Sun, and J. Shen, "Assembly of alternating TiO_2/CdS nanoparticle composite films," *Journal of Materials Chemistry*, vol. 8, no. 6, pp. 1327–1328, 1998.

[16] M. G. Kang, H.-E. Han, and K.-J. Kim, "Enhanced photodecomposition of 4-chlorophenol in aqueous solution by deposition of CdS on TiO_2," *Journal of Photochemistry and Photobiology A: Chemistry*, vol. 125, no. 1–3, pp. 119–125, 1999.

[17] J.-S. Hu, Y.-G. Quo, H.-P. Liang, L.-J. Wan, C.-L. Bai, and Y.-G. Wang, "Interface assembly synthesis of inorganic composite hollow spheres," *Journal of Physical Chemistry B*, vol. 108, no. 28, pp. 9734–9738, 2004.

[18] S. V. Tambwekar, D. Venugopal, and M. Subrahmanyam, "H_2 production of (CdS-ZnS)-TiO_2 supported photocatalytic system," *International Journal of Hydrogen Energy*, vol. 24, no. 10, pp. 957–963, 1999.

[19] W.-W. So, K.-J. Kim, and S.-J. Moon, "Photo-production of hydrogen over the CdS-TiO_2 nano-composite particulate films treated with $TiCl_4$," *International Journal of Hydrogen Energy*, vol. 29, no. 3, pp. 229–234, 2004.

[20] H. Fujii, K. Inata, M. Ohtaki, K. Eguchi, and H. Arai, "Synthesis of TiO_2/CdS nanocomposite via TiO_2 coating on CdS nanoparticles by compartmentalized hydrolysis of Ti alkoxide," *Journal of Materials Science*, vol. 36, no. 2, pp. 527–532, 2001.

[21] Ö. E. Kartal, M. Erol, and H. Oğuz, "Photocatalytic destruction of phenol by TiO_2 powders," *Chemical Engineering and Technology*, vol. 24, no. 6, pp. 645–649, 2001.

[22] G. W. Robertson and C. N. Satterfield, "Effectiveness factor for porous catalysts. Langmuir-hinshelwood kinetic expressions," *Industrial & Engineering Chemistry Fundamentals*, vol. 4, no. 3, pp. 288–293, 1965.

[23] G. W. Robertson and C. N. Satterfield, "Effectiveness factor for porous catalysts. Langmuir-hinshelwood kinetic expressions for bimolecular surface reactions," *Industrial & Engineering Chemistry Fundamentals*, vol. 5, no. 3, pp. 317–325, 1966.